Optimization of a Scroll Compressor for Liquid Flooding

Ian H. Bell[a,*], Eckhard A. Groll[a], James E. Braun[a], Galen B. King[a], W. Travis Horton[a]

[a]*Purdue University Department of Mechanical Engineering, 140 S. Martin Jischke Drive, West Lafayette, IN, 47906*

Abstract

In two companion papers, simulation models for the working processes of liquid-flooded scroll compressors and expanders have been developed and validated against experimental data. In this study, analytic models are presented for the modes of irreversibility generation in the liquid-flooded scroll compressor including built-in volume ratio maladjustment, pressure drop and leakage. A thermodynamic model is used to derive the ideal volume ratio for a liquid-flooded compressor, which is higher than that of dry compression. An optimum set of built-in volume ratio and scroll base circle radius is found which maximizes the overall isentropic efficiency by minimizing the leakage and pressure drop irreversibilities. The irreversibility generation models are used to optimize a scroll compressor for the Liquid-Flooded Ericsson cycle application. The model predicts scroll compressor overall isentropic efficiency of over 80% (based on the shaft power) at an oil mass fraction of 88%.

Key words:
scroll compressors, liquid flooding, isothermal compression, optimization, high efficiency

1. Introduction

Scroll compressor performance optimization is a complex endeavor because many parameters affect the performance of the scroll compressor. A significant amount of information is required to make an intelligent optimization. Selection of the optimal design parameters is complicated by the fact that many of the design parameters are tightly coupled together. Some of the important design parameters that govern the compressor efficiency are

- Scroll wrap geometry
- Internal heat transfer coefficient
- Motor & mechanical losses
- Leakage gap widths
- Pressure drops

In the open literature, there is little formalized analysis for the optimization of scroll compressor efficiency, and none for scroll compressors with liquid flooding. One of the major reasons for this paucity of design optimization information is the highly proprietary nature of scroll compressors. In particular, the details of the scroll compressor, such as leakage gap widths, cutting tool diameter, and motor efficiency are often not known *a priori*.

Bush et al. (1986) developed a framework for the analysis of the irreversibilities in the scroll compressor, the first step for the optimization of the compressor. Etemad et al. (1989) presented a method for optimization of the compressor and discussed all of the important parameters that enter into the design. Detailed results were not provided. Liu et al. (2010) carried out a detailed optimization of the scroll compressor frictional losses, and included enough information on the compressor design to fully characterize the scroll machine and its losses.

The analysis presented here for a scroll compressor with liquid flooding is focused on the optimization of the compressor by decreasing three main irreversibilities - leakage losses, pressure drop, and under- or over-compression losses due to built-in volume ratio maladjustment. A detailed analysis of the effects of motor and mechanical losses is not included as it is beyond the scope of this study.

2. Definition of Irreversibility Terms

The irreversibilities generated in the compressor are ultimately responsible for the deviation from the ideal working process for the scroll compressor. Bush et al. (1986) derived simple models for each of the irreversibilities in the scroll compressor based on scaling laws using empirical coefficients. The evaluation of the irreversibilities generated in the compression process in a reciprocating compressor has been developed by McGovern et al. (1992). Wagner et al. (1994) present a means of calculating the exergetic losses in the compression process based on the conservation of exergy for each control volume. This framework allows for the calculation of the total irreversibility, but does not allow the tracking of the provenance of each portion of the total irreversibilities.

*Corresponding Author
Email addresses: ian.h.bell@gmail.com (Ian H. Bell), groll@purdue.edu (Eckhard A. Groll), jbraun@purdue.edu (James E. Braun), kinggb@purdue.edu (Galen B. King), wthorton@purdue.edu (W. Travis Horton)

Based on the model presented in the companion paper (Bell et al., 2012a), the working process of the scroll compressor is determined. Based on the working process, the average irreversibilities over the course of a rotation can be calculated. The following sections present mathematical models for the irreversibilities generated in the scroll compressor. The names of the control volumes are consistent with the nomenclature presented in the companion paper (Bell et al., 2012a).

2.1. Suction Losses

The ideal suction process is one in which there is no pressure drop between the suction line and the suction chamber, and the pressure of the suction chamber is always equal to that of the suction line while refrigerant is being drawn into the suction chamber. Any extra boundary work done during the suction process will result in more shaft power being required for the compressor. The irreversibilities generated from the extra boundary work due to suction pressure drops can be calculated by

$$\dot{\mathbf{E}}_{suction} = -f \int_{p<p_s} (p_s - p) \frac{dV}{d\theta} d\theta \tag{1}$$

where the contributions from both suction chambers are summed. The integral term is approximated by the use of trapezoidal integration. The parameter f is the frequency of the compressor in Hz.

2.2. Leakage Losses

During the compression process, refrigerant leaks from high pressure to low pressure through the flank and radial leakage gaps. The flow through each leakage path can be considered adiabatic. Since the leakage flow does not carry out any work, the difference in flow exergy is equal to the irreversibility generation for each flow path. Thus the total irreversibility generated from all leakage paths can be determined from

$$\dot{\mathbf{E}}_{leakage} = \sum_{flank,radial} \dot{m}(\mathbf{e}_{up} - \mathbf{e}_{down}) \tag{2}$$

where $\dot{m}$ is the mass flow rate through a given gap, and the specific flow exergy (neglecting kinetic and potential energy terms) is evaluated for the upstream and downstream states of the leakage path as

$$\mathbf{e}_f = (h - h_0) - T_0(s - s_0) \tag{3}$$

Properties without a subscript are evaluated at the given state point (either the upstream or downstream point of the leakage flow path), while those with the subscript "O" are evaluated at ambient temperature and pressure, taken here to be 298 K and 101.325 kPa respectively. Mixture properties as described in the companion paper (Bell et al., 2012b) are used throughout.

2.3. Mechanical Losses

The mechanical losses of the scroll compressor also contribute to additional shaft power. As described in the companion paper (Bell et al., 2012b), the mechanical losses can be expressed with a constant loss torque as proposed by Yanagisawa (2001).

$$\dot{\mathbf{E}}_{mechanical} = \omega \tau_{loss} \tag{4}$$

2.4. Discharge Losses

At the discharge angle, the compression chambers begin to open to the fluid in the discharge region. If the pressure of the fluid in the compression chambers at the discharge angle is greater than the discharge pressure, irreversibilities are generated due to throttling of the fluid to the discharge pressure, as well as the additional boundary work required to compress the fluid due to the higher pressure. This case is referred to as over-compression. On the other hand, if the pressure of the compression chambers is below the discharge pressure at the discharge angle, back flow from the discharge region to the compression chambers occurs to bring the fluid in the compression chambers to the discharge pressure. This case is referred to as under-compression. The flow area between compression chambers and the discharge region opens slowly, which results in a relatively gentle pressure equilibration process. As a result, scroll compressors are somewhat less sensitive to undercompression than other types of compressors.

In either case of under-compression or over-compression, the total initial volume of the compression and discharge chambers at the beginning of the discharge process is defined as

$$V_a = V_{c1} + V_{c2} + V_{dd} \tag{5}$$

and an effective initial pressure is defined as the volume-weighted pressure of the chambers, or

$$p_a = \frac{p_{c1} \cdot V_{c1} + p_{c2} \cdot V_{c2} + p_{dd} \cdot V_{dd}}{V_a} \tag{6}$$

In the case of over-compression, the ideal boundary work is obtained from a constant pressure process at the discharge pressure from the initial discharge volume V_a to the clearance volume V_{cl}. Thus, the ideal work for one revolution in the case of over-compression is defined by

$$W_{ideal,OC} = -p_d(V_{cl} - V_a) \tag{7}$$

In the case of under-compression, the ideal discharge process is an adiabatic compression process from (p_a, V_a) to (p_d, V_b) and then, a constant pressure process at the discharge pressure from V_b to V_{cl}. The intersection volume V_b can be obtained from

$$V_b = V_a \left(\frac{p_a}{p_d} \right)^{1/k^*} \tag{8}$$

where k^* is the ratio of mixture specific heats given by

$$k^* = \frac{x_l c_l + (1 - x_l) c_{p,g}}{x_l c_l + (1 - x_l) c_{v,g}} \tag{9}$$

Thus, the ideal boundary work for the under-compression case can be given by

$$W_{ideal,UC} = \frac{p_a \cdot V_a - p_b \cdot V_b}{1.0 - k^*} - p_d(V_{cl} - V_b) \qquad (10)$$

which neglects the work of compression of the oil, assumes the entire volume to be gas, and treats the gas as being an ideal gas. Thus the actual discharge chamber boundary work can be calculated from

$$W_{actual} = \sum_{d1,d2,dd,ddd} \left[-\int_0^{2\pi} p \frac{dV}{d\theta} d\theta \right] \qquad (11)$$

Yielding the actual discharge irreversibility of

$$\dot{\mathbf{E}}_{discharge} = f\left(W_{actual} - W_{ideal}\right) \qquad (12)$$

where W_{ideal} is either $W_{ideal,UC}$ or $W_{ideal,OC}$ for under-compression and over-compression respectively.

2.5. Adiabatic Power

The adiabatic compression power of the refrigerant-liquid mixture can be defined by

$$\dot{W}_{adiabatic} = \dot{m}_{total}(h_d|_{s=s_s} - h_s) \qquad (13)$$

where $h_d|_{s=s_s}$ is the mixture enthalpy at the discharge pressure and the suction entropy, and $\dot{m}_{total}$ is the total mass flow rate of oil and gas passing through the scroll compressor.

2.6. Other Losses

The analysis presented above to determine the irreversibility generation neglects the irreversibilities associated with heat transfer over a finite temperature difference, both from the scroll wraps to the fluid, as well as from the scroll compressor shell to the ambient. In practice, the heat transfer is a result of the other irreversibilities. As shown below, neglecting heat transfer does not appear to have a significant impact on the overall accuracy of the irreversibility generation modeling.

2.7. Validation of Losses

Theoretically, if all losses are properly accounted for, the sum of the adiabatic compression power, the heat transfer rate to the ambient, and the irreversibility terms should equal the experimentally-measured shaft power. For the experimental data and computer modeling results from the companion paper (Bell et al., 2012b), Figure 1 shows the sum of the adiabatic power, the irreversibility terms, and the heat transfer rate to the ambient versus the experimentally measured shaft power. The losses are well quantified using the above analysis since both power terms agree within 3% of the experimentally-measured shaft power for all points.

Once the scroll compressor model has been validated and tuned with the use of experimental data from the companion paper (Bell et al., 2012b), it is then possible to determine the distribution of irreversibilities for each experimental operating point. Table 1 shows the losses for each run of the model, where the run numbers correspond to those from the companion paper (Bell et al., 2012b). In each set of three data points (1 to 3, 4 to 6, etc...), the pressure ratio is effectively constant, and the oil mass fraction is decreased. From these results, it can be shown that the suction and discharge irreversibilities decrease as the oil mass fraction decreases. In addition, the leakage irreversibilities decrease due to the decrease in suction and discharge pressure drops. This decrease in suction and discharge pressure drops result in a lower mean pressure difference over each leakage gap, and therefore, less leakage flow rate and less irreversibility generation.

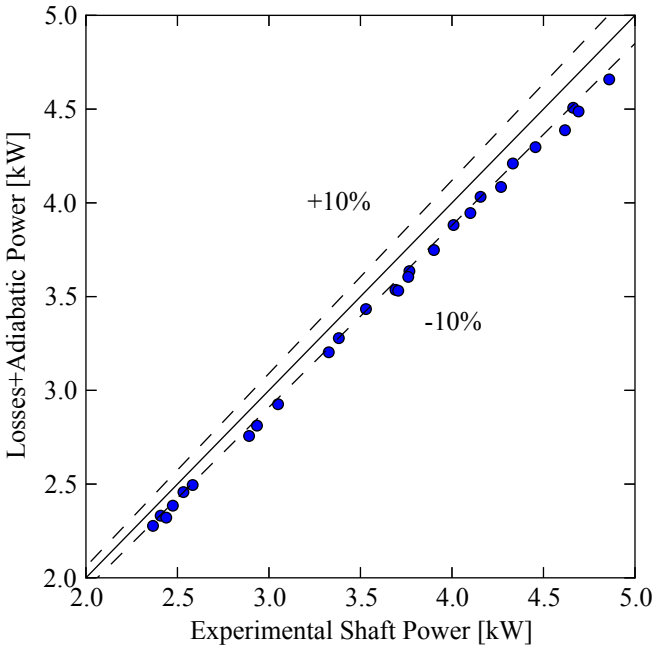

Figure 1: Summation of losses plus adiabatic compression power versus shaft power predicted from model for points from Ericsson cycle testing

3. Optimization for Ericsson Cycle Optimal Design Point

From the analysis of Hugenroth et al. (2006) it was found that there exists an optimal operation point for the Liquid-Flooded Ericsson Cycle (LFEC) that yields the maximum cycle Coefficient of Performance (COP is the ratio of cooling capacity to net input power). In order to achieve the desired COP of 1.25, suction and discharge pressures of 500 kPa and 1850 kPa respectively are used with an assumed compressor adiabatic efficiency of 87%. This is a very challenging target for compressor design. In this section, a method is proposed for carrying out the optimization process to approach this target efficiency. While the optimization process of Hugenroth et al. (2006) was

Table 1: Irreversibility generation components for each experimental testing point from LFEC experimental testing

Run	p_r	x_l	$\dot{W}_{ad}$	Rad.	Flank	Suct.	Disc.	Mech.
#	-	-	kW	kW	kW	kW	kW	kW
1	3.04	0.91	1.55	0.08	0.08	0.17	0.24	0.35
2	3.04	0.83	1.59	0.07	0.07	0.10	0.18	0.35
3	3.03	0.70	1.61	0.06	0.06	0.06	0.15	0.35
4	2.74	0.86	2.32	0.15	0.15	0.18	0.31	0.35
5	2.69	0.74	2.34	0.13	0.13	0.11	0.24	0.35
6	2.67	0.60	2.35	0.12	0.12	0.08	0.21	0.35
7	2.54	0.81	2.90	0.22	0.20	0.19	0.38	0.35
8	2.48	0.69	2.91	0.20	0.18	0.13	0.31	0.35
9	2.45	0.53	2.91	0.18	0.17	0.09	0.28	0.35
10	3.30	0.91	1.57	0.09	0.09	0.17	0.25	0.35
11	3.27	0.83	1.63	0.07	0.08	0.10	0.18	0.35
12	3.29	0.64	1.66	0.07	0.07	0.05	0.15	0.35
13	2.76	0.84	2.68	0.19	0.18	0.19	0.33	0.35
14	2.79	0.74	2.62	0.17	0.16	0.12	0.25	0.35
15	2.83	0.59	2.61	0.16	0.15	0.08	0.22	0.35
16	2.70	0.81	3.14	0.25	0.24	0.19	0.36	0.35
17	2.60	0.69	3.12	0.22	0.21	0.13	0.30	0.35
18	2.66	0.54	3.03	0.20	0.18	0.09	0.26	0.35
19	3.23	0.90	1.94	0.11	0.12	0.17	0.27	0.35
20	3.14	0.81	1.98	0.10	0.10	0.10	0.20	0.35
21	3.12	0.68	2.01	0.09	0.09	0.07	0.18	0.35
22	2.98	0.86	2.58	0.18	0.18	0.19	0.31	0.35
23	2.90	0.75	2.61	0.16	0.16	0.12	0.25	0.35
24	2.87	0.61	2.62	0.15	0.15	0.08	0.22	0.35
25	2.80	0.82	3.27	0.27	0.26	0.20	0.36	0.35
26	2.73	0.70	3.28	0.24	0.23	0.13	0.30	0.35
27	2.69	0.55	3.28	0.23	0.21	0.09	0.27	0.35

based on a smaller cooling capacity, here the suction displacement volume is fixed to be equal to that of the compressor used in the experimental testing of the companion paper (Bell et al., 2012b). The optimization process begins with the compressor from the LFEC testing. The compressor inlet temperature is fixed at 5°C as the cool thermal reservoir for the LFEC is set at 2°C. For Zerol 60 (an alkylbenzene refrigeration oil) and nitrogen as the working fluid pair, from analytical studies Hugenroth found the optimal ratio of oil capacitance rate to gas capacitance rate to be 12.47, or an oil mass fraction of 88%. The capacitance rate is defined as the product of the mass flow rate and the constant-pressure specific heat of the given phase. In spite of the large mass fraction of oil, at the inlet of the compressor the gas still occupies 95% by volume (based on homogeneous void fraction) because of the large difference in densities between the oil (865 kg m^{-3}) and the gas (6 kg m^{-3}).

3.1. Analysis of Existing Losses

A systematic procedure is carried out in order to minimize the irreversibilities defined in the previous section. Figure 2 shows the pressures in the baseline compressor

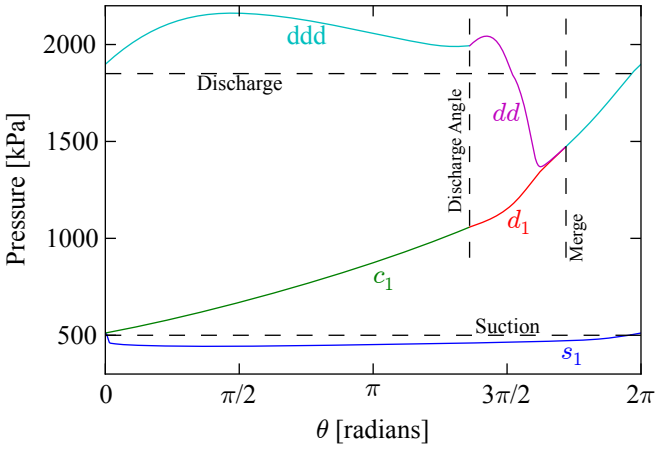

Figure 2: Pressures in baseline compressor at the LFEC optimal operation point (simulation results)

chambers over the course of one rotation. The ideal working process for the scroll compressor is a suction process where the suction pocket is filled at the suction pressure, a compression process that compresses the fluid all the way to the discharge pressure, and a discharge process where the fluid is discharged at the discharge pressure. The baseline compressor does not exhibit a working process that resembles the ideal compression process.

In both the suction and discharge processes, there are significant pressure drops due to the combination of a large mass flux of oil, small discharge port and a flow path which is not sufficiently straight. With 88% oil by mass passing through the discharge port, the effective density of the fluid at the discharge port is increased by more than seven times over the flow of pure nitrogen. The commensurate seven-fold increase in mass flux is the main driver for the large discharge pressure drop. The same effect is seen at the suction port.

The other irreversibility that can be readily visualized on the pressure-crank angle plot is the mal-adjustment of the built-in volume ratio for the imposed pressure ratio. With the built-in volume ratio of 1.61, the pressure of the compression chambers at the discharge angle is only 1057.2 kPa while the imposed discharge pressure is 1850 kPa. The inability of the scroll wraps to sufficiently compress the fluid results in under-compression losses. The flow resistance of the oil and gas attempting to flow back to equalize pressure with the compression chambers means that oil-flooded compressors suffer less from under-compression losses than non-flooded scroll compressors.

Figure 3 shows the losses of the scroll compressor with liquid flooding at the LFEC design point from which it is shown that approximately 78% of the losses arise from sources other than mechanical losses. These non-mechanical losses can be mitigated through proper design of the scroll machine.

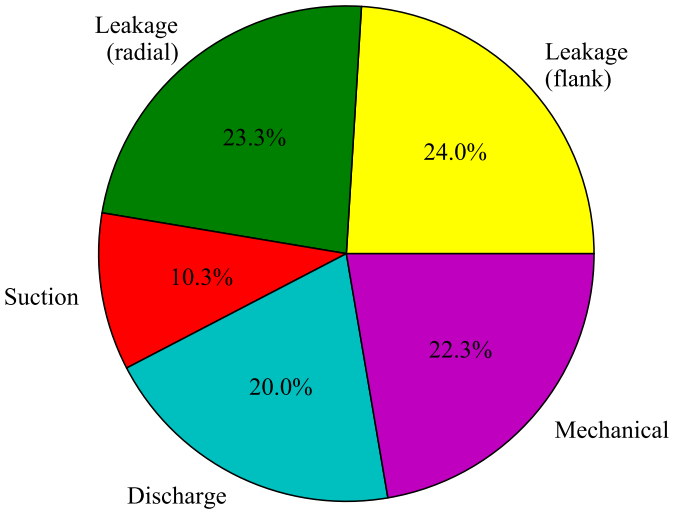

Figure 3: Distribution of Losses for baseline compressor

4. Optimization

As identified above, the readily corrected losses can be grouped into four categories - discharge losses, suction losses, mechanical losses, and leakage losses. A three-step process is proposed here to optimize the compressor's performance. First the suction and discharge pressure drops are decreased by increasing the flow areas, then the under-compression losses are decreased by increasing the volume ratio, and finally the leakage losses are decreased by decreasing the leakage gap widths. The configurations tested are

A. Baseline system
B. Larger suction and discharge port with single arc to close involutes
C. Larger volume ratio
D. Larger volume ratio with less leakage

4.1. Assumptions and Constraints

In order to carry out the optimization process, the following constraints were imposed on the compressor:

- Displacement of compressor held constant at 104.8 cm^3 (same as baseline compressor).
- Thickness of scroll wrap held constant at 4.66 mm (same as baseline compressor) in order to ensure that the scroll wraps are sufficiently stiff to handle the mechanical load.
- Mechanical efficiency of compressor held constant at 90%. In practice the mechanical efficiency of the scroll compressor will also be impacted by the particulars of the scroll geometry and its construction. 90% is believed to be a reasonable estimate of the mechanical efficiency possible based on the data from the companion paper (Bell et al., 2012b). Other researchers have also demonstrated mechanical efficiencies on the order of 90% (Ishii et al., 1990). The mechanical losses can be obtained from the mechanical efficiency η_m by

$$\dot{W}_{ML} = \frac{1-\eta_m}{\eta_m}\dot{W}_{mix} \tag{14}$$

where $\dot{W}_{mix}$ is the mixture compression power defined in the companion paper. The loss torque τ_{loss} can be defined by

$$\tau_{loss} = \dot{W}_{ML}/\omega \tag{15}$$

4.2. Suction and Discharge Geometry

The compressor used in this study has a relatively small discharge port with a diameter of 12 mm for the large quantity of oil flow that is discharged through it. Thus, the first step considered to optimize the scroll compressor is an increase in the discharge port diameter. Another factor which negatively impacts the pressure drop from the discharge region is blockage of the discharge port which occurs due to the tip of the orbiting scroll. Finally, the circuitous path the oil-gas mixture must take to exit the compressor shell results in a further pressure drop. First the baseline scroll compressor is modified to use two arcs to close the involute pair at the discharge in order to decrease the amount of discharge port blockage which occurs over one rotation. The radius of the smaller arc is equal to 1.0 mm. In addition, the discharge port is increased in size to the largest diameter that still fits into the discharge region, as seen in Figure 4. This yields a discharge port of 24 mm. Bell (2011) provides the solutions for the geometry for the curves used for the discharge region. The free discharge port area can be calculated using a numerical integration scheme, and the two discharge port configurations can be seen in Figure 5. Finally, the discharge area correction term presented in the companion paper is removed. The physical meaning of this removal is the substitution of a smooth pipe for the circuitous flow in the discharge plenum, resulting in a significant decrease in the discharge pressure drop. When there are significant under-compression losses, smaller discharge ports can be beneficial to decrease the under-compression losses, but small discharge ports also result in large pressure drops during the outflow part of the rotation. The goal of the optimization is to increase the volume ratio to greatly decrease the discharge pressure drop. Thus, the largest discharge port possible was used.

As shown in Figure 2, there is a large amount of irreversibilities due to the pressure drops in the suction process. As described in the companion paper (Bell et al., 2012a), the flow entering the compressor must change direction in order to enter the suction pockets. In a practical compressor, this problem can be remedied by increasing the diameter of the suction ports as well as splitting the flow into two streams, each of which inject directly into the suction pocket without a change in direction. In order to account for having two separate suction ports for the compressor, the area correction term, which was included

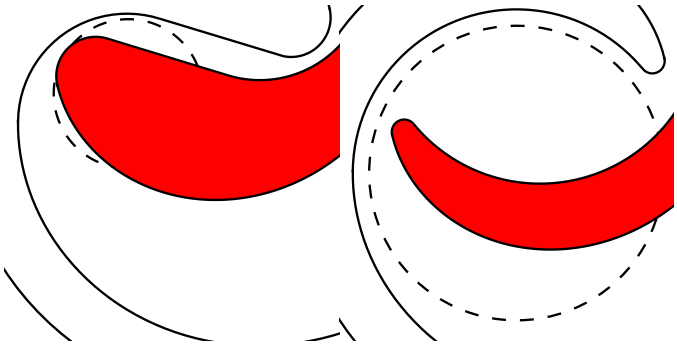

Figure 4: Port blockages at $\theta = 7\pi/4$ for baseline compressor (left) and 2 arc discharge with larger discharge port (right)

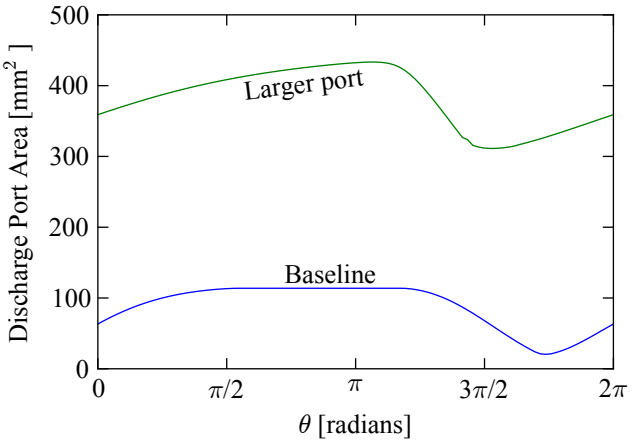

Figure 5: Port free area over one rotation

in the suction flow model to account for the pressure drop due to the bends, is removed. In addition, the inlet flow area was set to be equal to double the inlet flow area of the baseline compressor. The pressure-crank angle plot for this system is shown in Figure 6.

From this figure it can be seen that the suction and discharge port pressure drop components have been successfully controlled using the modifications presented here, though there are still two major irreversibilities remaining, the under-compression and leakage losses.

4.3. Derivation of ideal volume ratio with liquid flooding

The volume ratios needed for liquid-flooded scroll compressors are in general greater than those without liquid flooding. In order to derive the volume ratio required for the liquid-flooded compression process, the following constraints are imposed:

- Adiabatic efficiency of compression process given by η_a
- Initial and final masses are equal
- Initial and final oil mass fractions are equal
- Homogeneous mixture properties are employed, as described in the companion paper (Bell et al., 2012b)

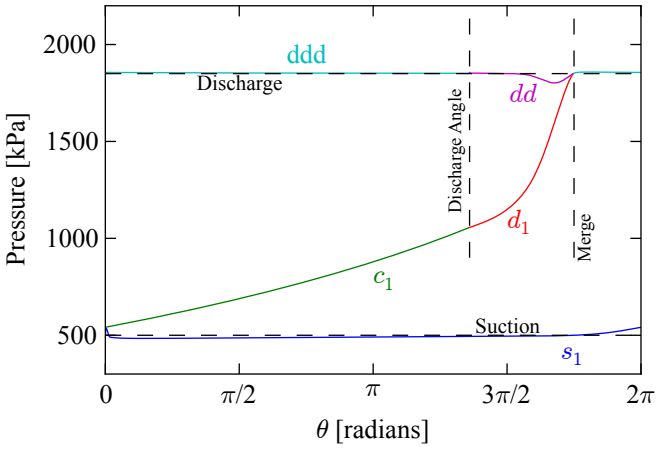

Figure 6: Pressure versus crank angle for two-inlet compressor (simulation results)

- Inlet condition (T_1, p_1, x_l) and discharge pressure p_2 imposed

Since the inlet state is known, the mixture properties at the inlet (h_1, ρ_1, s_1) can be obtained from the mixture model. The isentropic outlet temperature can be obtained from the equation

$$s_m(T_{2s}, p_2, x_l) = s_1 \tag{16}$$

where T_{2s} is iteratively determined using a numerical solver. The isentropic enthalpy is obtained from

$$h_{2s} = h_m(T_{2s}, p_2, x_l) \tag{17}$$

and based on the definition of the adiabatic efficiency, the outlet enthalpy is obtained from

$$h_2 = \frac{h_{2s} - h_1}{\eta_a} + h_1 \tag{18}$$

which allows to solve for the actual discharge temperature T_2 from

$$h_m(T_2, p_2, x_l) = h_2 \tag{19}$$

With T_2 known, the density at state point 2 (ρ_2) can be obtained.

Conservation of mass for the compression process can be expressed as

$$\rho_1 V_1 = \rho_2 V_2 \tag{20}$$

and thus, if V_{ratio} is defined by $V_{ratio} = V_1/V_2$, then V_{ratio} can be given by

$$V_{ratio} = \frac{\rho_2}{\rho_1} \tag{21}$$

Figure 7 shows the results of the analysis presented in this section for the design point of the Liquid-Flooded Ericsson Cycle, which will be described further below. For adiabatic reversible compression (η_a=1), the required volume ratio increases as the oil mass fraction increases, but

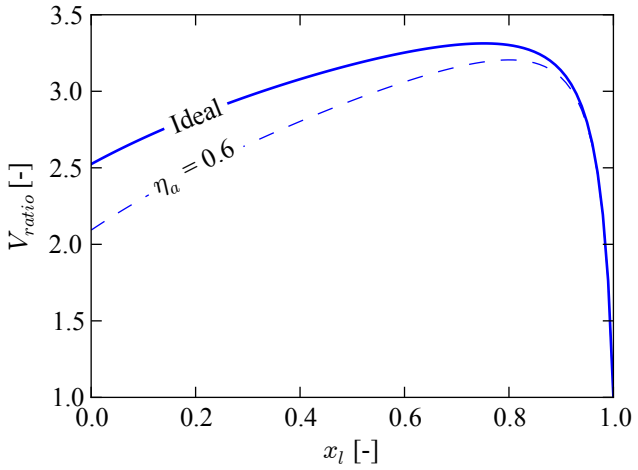

Figure 7: Ideal volume ratio as a function of oil mass fraction for operation at the LFEC optimal operation point.

at high oil mass fractions, the volume ratio goes to unity. When there is no oil-flooding (x_l=0), the ideal volume ratio can be found from the compression of pure gas. In the limit that the oil mass fraction goes to 1, the volume ratio does as well. This is due to the fact that for an incompressible fluid, an infinitely small decrease in volume is required to obtain an infinitely large increase in pressure.

4.4. Derivation of geometric parameters

The analysis of the geometry of the scroll compressor is quite complex. A simplified treatment of scroll compressor geometry will be presented here, but a comprehensive analysis of the scroll compressor geometry can be obtained from Bell (2011), including derivation of the terms employed here. The scroll compressor is composed of two scroll wraps which are symmetric and are in contact at a number of points. One scroll wrap is fixed, and the other orbits around the fixed scroll. The fixed scroll itself is composed of two involute curves. Figure 8 shows the geometry of the fixed scroll. The inner and outer involute curves have initial involute angles of ϕ_{i0} and ϕ_{o0} respectively on the base circle of radius r_b. The involutes exist between the involute angles ϕ_{is} and ϕ_{ie} on the inner involute and ϕ_{os} and ϕ_{oe} on the outer involute.

In order to decrease under-compression losses, it is necessary to increase the built-in volume ratio so that the gas-liquid mixture is compressed nearer the discharge pressure before the compression pocket opens to the discharge pressure. Thus the geometry of the scroll wraps must be modified to yield a larger volume ratio. In order to achieve a larger volume ratio while imposing several other parameters, the following constraints were set:

- Inner scroll wrap initial angle held at 0.0. The inner involute initial angle is a free parameter, which yields a family of identical, but rotated, scroll wraps. 0.0 is used for simplicity, though in practice, the value of one of the involute initial angles can be freely selected.

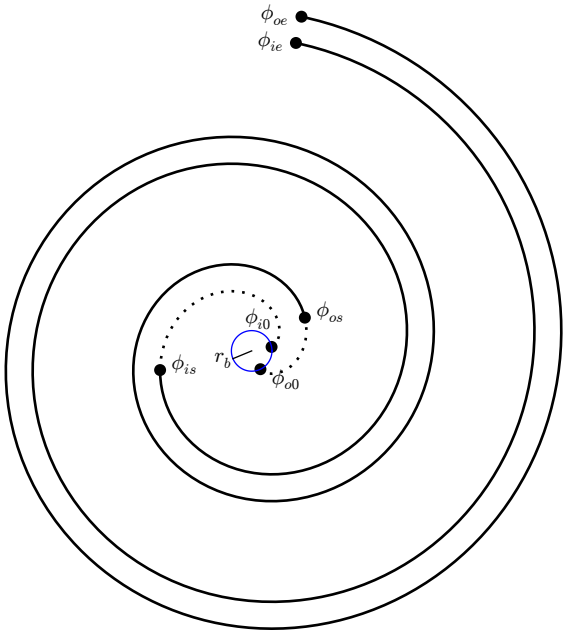

Figure 8: Fixed scroll involute geometry.

- Inner scroll wrap starting angle given by ϕ_{is}=ϕ_{i0}+π. An offset of π radians between inner initial and inner starting angles yields a reasonably open discharge region which allows for a large discharge port.

- Outer scroll wrap starting angle given by ϕ_{os}=ϕ_{is}-π+0.3.

The displacement is constant, where the displacement of the compressor is given by

$$V_{disp} = -2\pi h_s r_b r_o \left(3\pi - 2\phi_{ie} + \phi_{i0} + \phi_{o0}\right) \tag{22}$$

In addition, the built-in volume ratio is given by

$$V_{ratio} = \frac{V_{disp}}{2V_{c,d}} = \frac{3\pi - 2\phi_{ie} + \phi_{i0} + \phi_{o0}}{-2\phi_{os} - 3\pi + \phi_{i0} + \phi_{o0}} \tag{23}$$

where $V_{c,d}$ is the volume of one of the innermost compression chambers at the discharge angle. The thickness of the scroll wrap is given by:

$$t = r_b(\phi_{i0} - \phi_{o0}) \tag{24}$$

and the orbiting radius is given by

$$r_o = r_b\pi - t \tag{25}$$

If the displacement V_{disp}, volume ratio V_{ratio} and thickness of the scroll wraps t are imposed, then there are three equations(22, 23, 25) and 6 unknowns (ϕ_{ie}, ϕ_{i0}, ϕ_{o0}, ϕ_{os},

h, r_b). Therefore, with the additional constraints imposed above(ϕ_{i0}=0, ϕ_{os}=0.3), there remains just one free variable, which can either be taken to be the scroll wrap height h_s or the base circle radius r_b. In this study, the base circle radius was taken as the free variable. A method for calculating the optimal base circle radius to minimize leakage is shown below.

With these constraints, it is possible to obtain an analytic solution for the relevant scroll wrap parameters. The outer involute initial angle is then given by

$$\phi_{o0} = -t/r_b \tag{26}$$

and after some algebra and simplification, the height is given by

$$h_s = \frac{V_{disp}}{2\pi r_b^2 V_{ratio}(\pi + \phi_{o0})(2\phi_{os} + 3\pi - \phi_{o0})} \tag{27}$$

and the ending angle of the scroll is given by

$$\phi_{ie} = \frac{V_{disp}}{4\pi h_s r_b^2(\pi + \phi_{o0})} + \frac{3\pi + \phi_{o0}}{2} \tag{28}$$

If another set of constraints is desired, it is possible to use a non-linear solver such as the one available in Engineering Equation Solver (EES) to obtain the scroll wrap geometry.

For the same volume ratio, scroll wrap thickness and displacement, the larger r_b is, the smaller h_s must be. This yields a family of solutions from a very narrow cylinder to a "pancake" scroll design. Selected members of this family are shown in Figure 9. All scroll wraps are plotted at the same scale.

4.5. Derivation of optimal base circle radius

As shown in the above section, for a given volume ratio, displacement, and scroll wrap thickness, a family of different scroll wraps can be obtained. The range of scroll wraps, from a narrow cylinder to a pancake scroll, offer different performances due to the variation in the leakage rates. It is therefore useful to develop a simple model for the leakage terms in order get a first guess for the optimal scroll wrap geometry from a leakage point of view. In the above analysis, the base circle radius r_b was a free variable, but the model presented here can predict the optimal base circle radius with reasonable accuracy.

To begin the analysis, it is first assumed that some portion of the scroll wrap does not contribute to radial leakage. This can be understood by considering the suction chamber. Over the course of the first rotation, the outermost conjugate point moves 2π radians towards the center of the compressor. Radial area between the suction chamber and the suction area does not contribute to leakage since there is effectively no pressure difference to drive the flow. Therefore, an effective ending angle of the scroll wrap is defined by

$$\phi_{ie}^* = \phi_{ie} - \pi \tag{29}$$

which removes the contribution of half of the suction chamber since over the course of one rotation, the mean conjugate angle is the inner ending angle minus a half rotation or π radians. The same argument is employed for the inner starting angle in the discharge region. Once the discharge region has equalized in pressure the radial leakage area no longer contributes to leakage. Therefore in the discharge region, another π radians are removed from the scroll involute, yielding an effective inner involute starting angle of

$$\phi_{is}^* = \phi_{is} + \pi \tag{30}$$

Thus the total radial leakage area based on the inner involutes of the fixed and orbiting scrolls can be given by

$$A_{radial}^* = 2\delta_r \int_{\phi_{is}^*}^{\phi_{ie}^*} r_b(\phi - \phi_{i0}) d\phi \tag{31}$$

which yields

$$A_{radial}^* = 2r_b\delta_r \left(\frac{(\phi_{ie}^*)^2}{2} - \frac{(\phi_{is}^*)^2}{2} \right) \tag{32}$$

because the inner initial angle ϕ_{i0} was fixed at 0 in order to derive the involute parameters.

The flank area is determined by the number of flank contact points in existence over the course of a rotation. The mean total number of flank contact points is given by

$$N_{flank} = 2\frac{\phi_{ie} - \phi_{is}}{2\pi} \tag{33}$$

and the flank leakage flow area for each contact point can be given by $h_s\delta_f$. Thus, the total flank leakage area is given by

$$A_{flank}^* = F\delta_f h_s N_{flank} \tag{34}$$

where F is a flow correction parameter. For a given flow area and pressure difference, more flow will go through the flank leakage. This can be understood by considering the hydraulic diameters of the leakage paths. In the radial leakage, the hydraulic diameter is always twice the gap width, while for the flank leakage, the conformal contact results in a hydraulic diameter that increases sharply away from the throat of the leakage path. As a result, the frictional effects for the radial leakage are more strongly felt than for the flank leakage. The ratio of flank to radial frictional leakage mass fluxes is approximated from their frictional flow models, and is given by a value for F near 3. This value was slightly tuned in order to better fit the results from the optimization carried out on the Liquid-Flooded Ericsson Cycle compressor presented in section 5 for a volume ratio of 2.7. In practice, the value of this ratio is dependent on the thickness of the scroll wrap and the system operating parameters, but since the purpose of this section is to derive a guess value for detailed optimization, this value is sufficiently accurate. Thus, the total effective leakage is given by

$$A_{total}^* = A_{radial}^* + A_{flank}^* \tag{35}$$

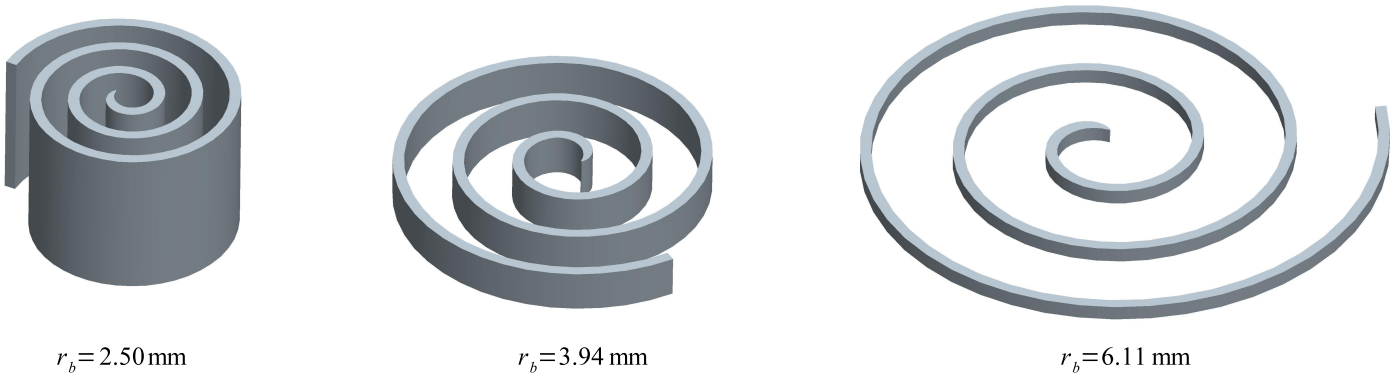

Figure 9: Family of scroll wraps for a volume ratio of 2.7 and a displacement of 104.8 cm^3

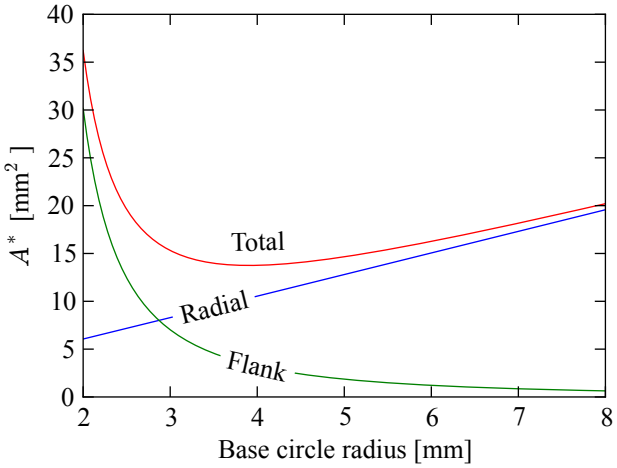

Figure 10: Effective flank and radial leakage areas for compressor with volume ratio of 2.7, displacement of 104.8 cm^3, scroll thickness of 4.66 mm.

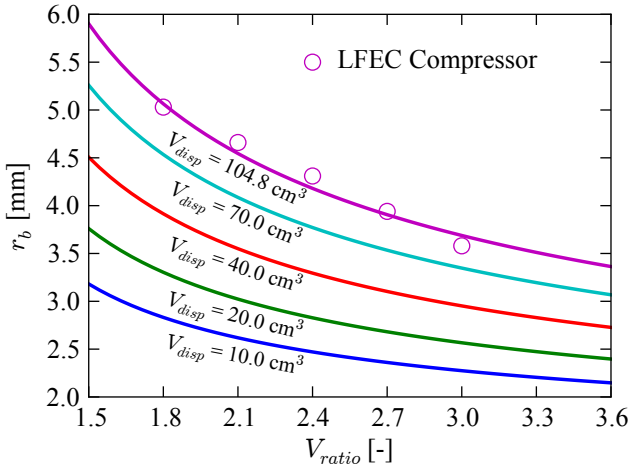

Figure 11: Optimal base circle radius as a function of volume ratio and displacement for a scroll thickness of 4.66 mm.

The results for the effective leakage areas as a function of base circle radius for a volume ratio of 2.7 and displacement of 104.8 cm^3 are shown in Figure 10. The effective radial leakage increases linearly with the base circle radius, while the effective flank leakage decreases with the base circle radius. Thus the sum of the two terms yields a minimum effective leakage area at a base circle radius of 3.91 mm.

Therefore it can be concluded that there is a base circle radius that optimizes the performance of the compressor by minimizing the effective leakage area. Thus a numerical optimization routine can be employed to determine the optimal base circle radius over a range of displacement and volume ratios for a fixed scroll wrap width of 4.66 mm. The results of this analysis are shown in Figure 11. The optimal base circle radii obtained from the detailed compressor modeling for the Liquid-Flooded Ericsson Cycle are also overlaid in order to demonstrate the effectiveness of this method for calculating an approximate optimal base circle radius. A similar plot can be generated for a different scroll wrap thickness. These results show that for a given displacement, as the volume ratio increases, the optimal base circle radius decreases. Furthermore, for a given volume ratio, as the displacement is increased, the optimal base circle radius increases. This chart can be generally employed in the design of scroll wraps, whether for flooded or dry compression applications. The inclusion of geometrically-dependent mechanical losses and scroll wrap manufacturing cost would result in different optimal scroll wrap geometries.

4.6. Compressor Analysis

Using the geometric analysis presented above, it is possible to construct a family of scroll compressors and use these parameters in the scroll compressor model to determine their performance for the optimal LFEC design point. The volume ratio is varied through the range 1.8 to 3.0 and the base circle radius is varied from 2.5 mm to 9.0 mm. Figure 12 shows the results from the compressor model for the LFEC design point. This figure shows that for a volume ratio of 1.8, the volume ratio is still insufficient to bring the oil-gas mixture to the discharge pressure. As a result, the under-compression losses result in maximum overall isentropic efficiency of 69% at

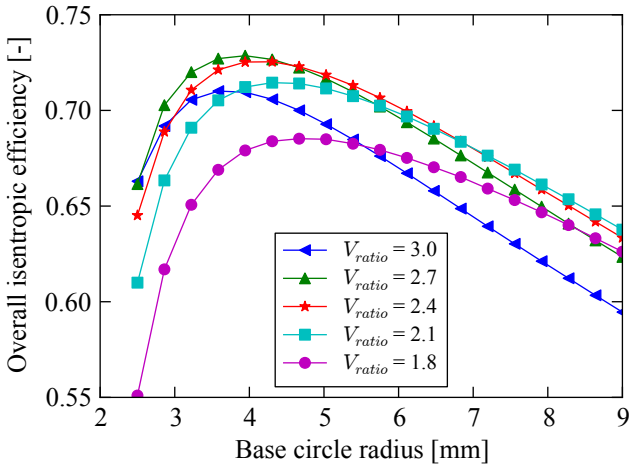

Figure 12: Overall isentropic efficiency of liquid-flooded scroll compressor as a function of volume ratio and base circle radius for a displacement of 104.8 cm^3

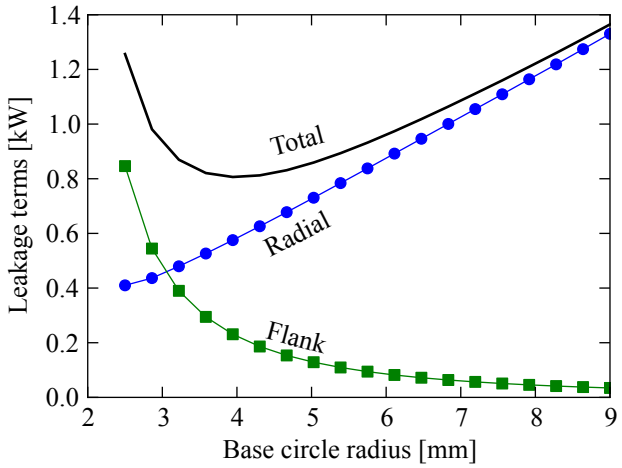

Figure 13: Leakage irreversibilities as a function of base circle radius for a volume ratio of 2.7 and displacement of 104.8 cm^3

a base circle radius of 5 mm. As the volume ratio is increased to 2.7, the overall isentropic efficiency also increases. Beyond a volume ratio of 2.7, there are significant over-compression losses since the mixture is compressed to beyond the discharge pressure at the discharge angle, and further increases in the volume ratio would result in more over-compression losses.

For each volume ratio, there is a base circle radius which maximizes the overall isentropic efficiency. Since the suction and discharge losses have been largely removed by the redesigns proposed here, the only remaining loss parameters are the leakage and the mechanical losses. Since the mechanical losses modeled here are independent of the compressor design, the leakages are the dominant terms impacting the compressor performance. For the same displacement and volume ratio, as the base circle radius goes to zero, the compressor becomes more and more cylindrical, resulting in the radial leakage area going to zero. In contrast, very small base circle radii result in large flank leakages due to the tall scroll wraps. Also, as the base circle radius goes to zero, the discharge port has to decrease in size because the discharge region area also scales with the base circle radius. In the limit that the base circle radius is very large, the scroll compressor becomes very flat and the flank leakage area goes to zero. As a result of the large base circle radius, the radial leakage area becomes very large.

For a given volume ratio and displacement, the base circle radius which minimizes the leakage losses also optimizes the overall isentropic efficiency. Figure 13 shows the radial, flank and total leakage irreversibilities for a volume ratio of 2.7. The base circle radius of 3.94 mm, or approximately 4.0 mm minimizes the leakage irreversibilities and also corresponds to the maximum overall isentropic efficiency.

Finally the leakage of the scroll compressor can be decreased by decreasing the tuned leakage gap widths. In order to achieve a real-world decrease in leakage gap width, significant redesign might be required. Such a redesign, for instance reducing the leakage gap widths from 12μm to 6μm, will have a significant impact on leakage losses. Figure 14 shows the overall isentropic efficiency of the compressor as a function of the leakage gap width. The same gap width is used for both flank and radial leakage. Of the modifications suggested up to this point, this is the modification which would be most difficult to achieve in practice. The 12 μm gap width was obtained from the tuning of the model for a compressor that was disassembled, had its radial compliance pinned, and was reassembled. Thus, using factory assembly it might be possible to achieve significantly smaller leakage gap widths under operation. A leakage gap width of 6 μm is used in the Ericsson Cycle analysis presented in the following section.

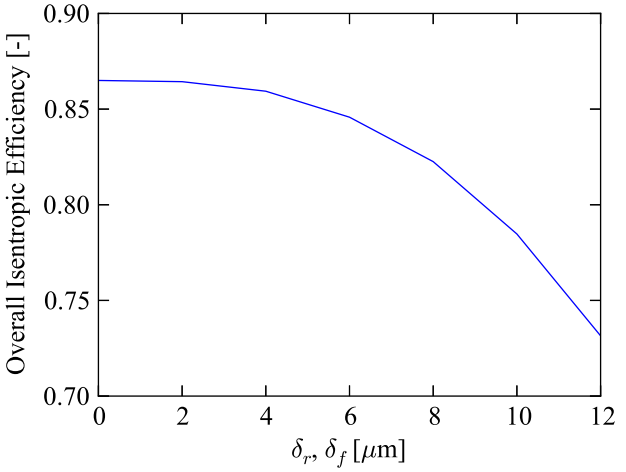

Figure 14: Overall isentropic efficiency of scroll compressor with liquid flooding as a function of leakage gap width for a volume ratio of 2.7 and circle radius of 3.94 mm

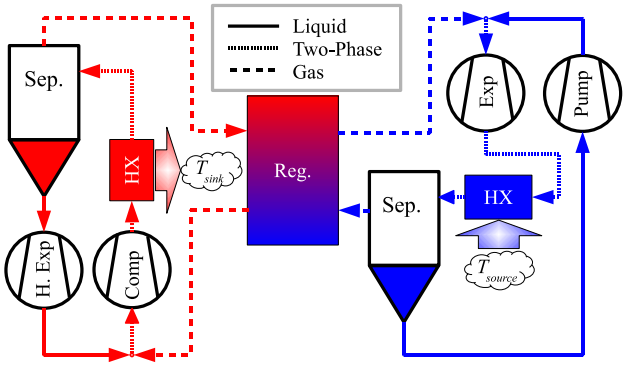

Figure 15: Schematic of Liquid-Flooded Ericsson Cycle Configuration

5. Liquid-Flooded Ericsson Cycle

The Ericsson Cycle is a theoretical gas refrigeration cycle that has isothermal compression and expansion processes and internal heat exchange. In its theoretical limit, this cycle yields the Carnot Coefficient of Performance, the best COP possible for a system pumping heat from a low temperature reservoir to a higher temperature reservoir. The challenge of this system is to achieve isothermal compression and expansion. Liquid-flooding of the compression and expansion processes has been proposed as a means of approaching the working processes of the Ericsson cycle.

In this section, the analysis of an Ericsson Cycle with the optimized liquid-flooded compressor is presented, and a schematic of the Liquid-Flooded Ericsson Cycle can be found in Figure 15. The analysis used here is based on the analysis developed by Hugenroth et al. (2007) to which the reader is directed for a description of the cycle modeling employed. The compressor model was run for 600 state points with inputs in the ranges:

- Inlet pressure (absolute) : 300 kPa to 700 kPa
- Pressure ratio : 1.5 to 4.5
- Oil Mass Fraction : 0.1 to 0.9
- Inlet temperature : 240 K to 300 K

The working fluids for the compressor model were nitrogen and alkyl-benzene oil respectively. A high-accuracy correlation for the compressor overall isentropic efficiency was fit to the compressor map data. This correlation is structured as the overall isentropic efficiency of the compressor as a function of the compressor suction temperature, suction pressure, pressure ratio and oil mass fraction. The volumetric efficiency of the flooded compressor was taken to be 100%. The motor efficiency for the compressor is assumed to be 95%

The compressor map was integrated into the Ericsson Cycle solver which is implemented in the Python programming language. A non-linear system solver is used to enforce the correct oil mass fraction entering the expander as well as the high-side pressure. Thus, for a set of source and sink temperatures, the model can predict the LFEC capacity and efficiency. The cycle parameters used in the modeling are given in Table 2. For a given set of source and sink temperatures, and imposed suction pressure and pressure ratio, the oil mass fractions passing through the compressor and expander can be freely varied. The performance of the LFEC cycle is highly dependent on the oil mass fractions selected through the hot and cold loops, and an optimizer can be used to maximize the system performance. The optimization of LFEC cycle efficiency is carried out using the L-BFGS-B optimization algorithm (Byrd et al., 1995) with an objective function of $1/COP$ and input parameters of oil mass fractions through the cold and hot sides of the system.

Table 2: Parameters for the Liquid-Flooded Ericsson Cycle Analysis.

Parameter	Value
T_{sink}	25 °C
Δp per component	0.0 kPa
η for Pump, Hyd. Expander, Expander	0.7
ε_{HX} for all HX	0.9

With a source temperature of 2°C, Figure 16 shows the second-law efficiency and cooling capacity as a function of suction pressure and pressure ratio. It can be seen that with no constraint on the capacity, the highest second-law efficiencies are found at low suction pressures, for a pressure ratio of approximately 3.2. This optimal pressure ratio is governed by the compressor geometry, in particular the built-in volume ratio. However, if the capacity is constrained to take on some finite value, perhaps 1.6 kW, there is suction pressure / pressure ratio pair which optimizes the cycle efficiency.

The optimal liquid mass fraction circulating through the compressor varies based on the applied pressures. Figure 17 shows contours of the optimal liquid mass fraction for the compressor for varied suction pressures and pressure ratios. For a given suction pressure, the ideal oil mass fraction increases as the pressure ratio increases.

While the LFEC struggles to achieve good efficiency at source temperatures near ambient, the LFEC system performance improves as the source temperature decreases. Figure 18 shows the second law efficiency and capacity overlaid for a source temperature of -50°C as a function of pressure ratio and compressor suction pressure. The second law efficiency is greatly improved with a relatively small decrease in capacity. The major challenge with such low source temperatures is finding a flooding liquid that can remain in the liquid phase at such low temperatures with a reasonably low viscosity.

6. Conclusion

Based on the work presented here, the following conclusions can be drawn:

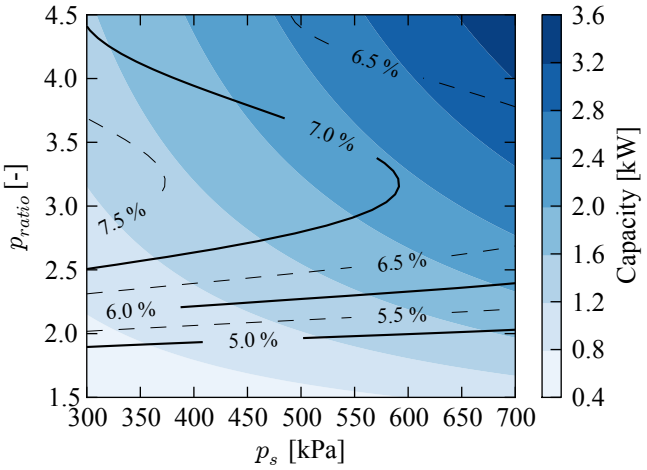

Figure 16: Second Law Efficiency (black contour lines) and capacity (filled contours) of LFEC with optimized oil mass fractions and a source temperature of 2°C

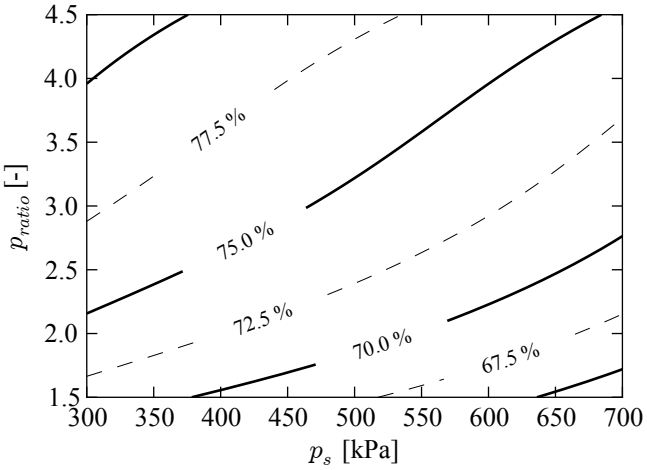

Figure 17: Optimal compressor oil mass fractions for LFEC with a source temperature of -50°C

- Analytic models have been developed for the irreversibilities during the compression process. The results of the model were validated using experimental data.
- Analytic models have been developed for the ideal volume ratio for compressors with varying amounts of liquid flooding.
- The design of the scroll compressor has been optimized for liquid flooding with a predicted overall isentropic efficiency of over 80%.
- The optimized scroll compressor was implemented in the Liquid-Flooded Ericsson Cycle numerical model yielding predictions of second-law efficiencies in cooling mode of up to 19% at a source temperature of -50 °C.

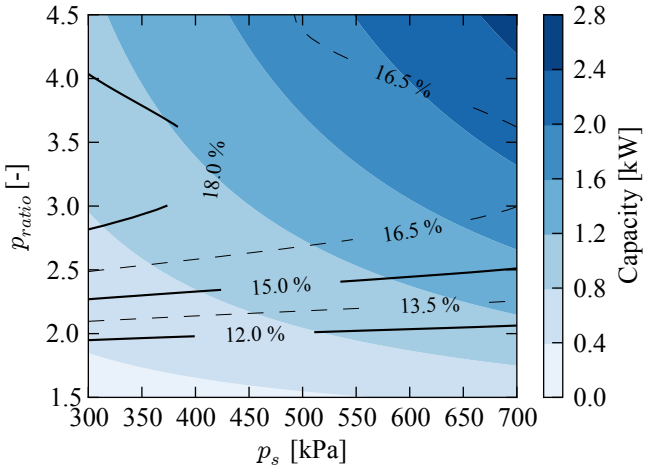

Figure 18: Second Law Efficiency (black contour lines) and capacity (filled contours) of LFEC with optimized oil mass fractions and a source temperature of -50°C

References

Bell, I., 2011. Theoretical and Experimental Analysis of Liquid Flooded Compression in Scroll Compressors. Ph.D. thesis, Purdue University.
URL `http://docs.lib.purdue.edu/herrick/2/`

Bell, I., Lemort, V., Groll, E., Braun, J., King, G., Horton, W. T., 2012a. Liquid-Flooded Compression and Expansion in Scroll Machines - Part I: Model Development. Int. J. Refrig. Submitted for Publication.

Bell, I., Lemort, V., Groll, E., Braun, J., King, G., Horton, W. T., 2012b. Liquid-Flooded Compression and Expansion in Scroll Machines - Part II: Experimental Testing and Model Validation. Int. J. Refrig. Submitted for Publication.

Bush, J. W., Caillat, J.-L., Seibel, S. M., 1986. Dimensional optimization of scroll compressors. In: 1986 International Compressor Engineering Conference at Purdue University.

Byrd, R. H., Lu, P., Nocedal., J., 1995. A Limited Memory Algorithm for Bound Constrained Optimization. SIAM Journal on Scientific and Statistical Computing 16, 1190–1208.

Etemad, S., Nieter, J., 1989. Design optimization of the scroll compressor. International Journal of Refrigeration 12 (3), 146 – 150.

Hugenroth, J., 2006. Liquid Flooded Ericsson Cycle Cooler. Ph.D. thesis, Purdue University.

Hugenroth, J., Braun, J., Groll, E., King, G., 2007. Thermodynamic analysis of a liquid-flooded Ericsson cycle cooler. Int. J. Refrig. 207, 331–338.

Ishii, N., Yamamura, M., Muramatsu, S., Yamamoto, S., Sakai, M., 1990. Mechanical Efficiency of a Variable Speed Scroll Compressor. In: 1990 Purdue Compressor Conference. pp. 192–199.

Liu, Y., Hung, C., Chang, Y., 2010. Design optimization of scroll compressor applied for frictional losses evaluation. International Journal of Refrigeration 33 (3), 615 – 624.

McGovern, J. A., Harte, S., 1992. Computer Simulation of Exergy Destruction within a Reciprocating Compressor. In: 1992 International Compressor Engineering Conference at Purdue University. No. 309-315.

Wagner, T. C., Deblois, R. L., Young, D. L., 1994. Energy and exergy analyses of the scroll compressor. In: 1994 International Compresor Engineering Conference at Purdue University. pp. 665–670.

Yanagisawa, T., Fukuta, M., Ogi, Y., Hikichi, T., 2001. Performance of an oil-free scroll-type air expander. In: Proc. Of the ImechE Conf. Trans. On compressors and their systems. No. C591/027/2001. pp. 167–174.

Nomenclature

Roman

c_l	Liquid specific heat (kJ kg^{-1} K^{-1})
$c_{p,g}$	Gas constant-pressure spec. heat (kJ kg^{-1} K^{-1})
$c_{v,g}$	Gas constant-volume spec. heat (kJ kg^{-1} K^{-1})
$\dot{\mathbf{E}}$	Rate of entropy generation (kW)
$\mathbf{e}$	Specific Exergy (kJ kg^{-1})
f	Frequency (s^{-1})
k^*	Effective ratio of specific heats (-)
h	Specific Enthalpy (kJ kg^{-1})
h_s	Height of the scroll (m)
p	Pressure (kPa)
p_r	Pressure ratio
r_o	Orbiting radius (m)
r_b	Base [generating] circle radius (m)
s	Specific Entropy (kJ kg^{-1} K^{-1})
t	Scroll wrap thickness (m)
T	Temperature (K)
V	Volume (m^3)
V_{disp}	Displacement volume (m^3)
V_{ratio}	Ratio of suction to discharge volumes (-)
V_1	Initial total volume (m^3)
V_2	Final total volume (m^3)
W	Work (kJ)
$\dot{W}_{gas}$	Gas compression power (kW)
$\dot{W}_{ML}$	Mechanical losses power (kW)
x_l	Oil mass fraction

Greek

β	Liquid void fraction (-)
δ	Leakage gap width (m)
ρ	Density (kg m^{-3})
ω	Rotational Speed (rad s^{-1})
τ_{loss}	Mechanical Loss Torque (kN m)
η_m	Mechanical Efficiency (-)
ϕ_{i0}	Inner scroll initial angle (radians)
ϕ_{is}	Inner scroll starting angle (radians)
ϕ_{ie}	Inner scroll ending angle (radians)
ϕ_{o0}	Outer scroll initial angle (radians)
ϕ_{os}	Outer scroll starting angle (radians)
ϕ_{oe}	Outer scroll ending angle (radians)

Subscripts

a	Initial total discharge chamber volume
b	Intersection discharge chamber volume
cl	Clearance
$c1$	The first compression chamber
$c2$	The second compression chamber
d	Discharge
$d1$	The first outer discharge chamber
$d2$	The second outer discharge chamber
dd	The central discharge chamber
ddd	The merged central discharge chamber
$down$	Downstream
f	Flank direction (along the scroll wrap)
r	Radial direction (across the scroll wrap)
s	Suction
$total$	Mixture (oil+gas)
up	Upstream
0	At the dead state